International Journal of Advances in Structural and Geotechnical Engineering

https://asge.journals.ekb.eg/

Print ISSN 2785-9509 *Online ISSN 2812-5142*

Special Issue for ICASGE'19

Behavior of tapered concrete filled double skin steel tubular short columns (CFDST)

Mahmoud El-Bogdadi, Omnia Kharoob, Mahmoud Abonagy

ASGE Vol. 04 (01), pp. 126-139, 2020

International Conference on Advances in Structural and Geotechnical Engineering

ICASGE'19

25-28 March 2019, Hurghada, Egypt

Behavior of tapered concrete filled double skin steel tubular short columns (CFDST)

Mahmoud El-Bogdadi[1], Omnia Kharoob[2], Mahmoud Abonagy[3]

[1] Associate Professor, Structural engineering department, Faculty of Engineering, Tanta University, Egypt. E-mail: mboghdadi@hotmail.com

[2]Associate Professor, Structural engineering department, Faculty of Engineering, Tanta University, Egypt. E-mail: omnia_m102010@yahoo.com

[3] Structural engineering department, Faculty of Engineering, Tanta University, Egypt E-mail: Mabonagy2012@gmail.com

ABSTRACT

Tapered concrete filled double skin steel tubular short columns CFDST has many advantages and widely used in the construction field. A finite element model has been made to simulate the behavior of tapered concrete filled double-skin steel tubular short columns and to be used in the parametric study. The behavior of tapered concrete filled double-skin steel tubular short columns CFDST has been studied in this research under the parameter of The concrete compressive strength *(fc***)** varied between 25 MPa to 40 MPa. The ratio of the internal tube thickness-to-outer tube thickness (t_i/t_o) varied from 0.63 to 1. The tapered angle (θ) varied from 0.5 degree to 1 degree. The ratio of the diameter of the internal tube-to-the diameter of the outer tube (d_i/D_o) varied from 0.25 to 0.88.

Keywords: Concrete, Tapered, steel, concrete filled, double skin.

1.INTRODUCTION

Composite columns have the advantages of reinforced concrete columns and steel columns together. It is widely used in modern high rise buildings because of its high compressive strength and seismic resistance compared with concrete columns. The composite columns are effective in resisting compression, tension and bending moment. In concrete filled the steel provide the confinement and support to concrete that increases the strength and ductility to the composite columns. The concrete-filled column has a special advantage as it does not need formwork or reinforcement. It is used bridges, storage tanks, and high rise building. A type of concrete-filled steel tubular columns CFST is the concrete filled double skin steel tubular columns CFDST which consists of an outer steel tube, inner steel tube, and concrete sandwich in between. This kind of composite columns has compressive strength more than the CFST because the outer tube provides confinement and the inner tube support the concrete sandwich too. To reduce the weight of CFST without affecting the capacity with different load cases the concrete filled double skin steel tubular columns CFDST became the solution. The CFDST has a similar behavior of CFST but the CFDST is lighter self-weight because of the hollow part inside the columns which will be a benefit in case of large sections. The CFDST has better damping characteristic and cycle performance because of the two steel tubes which provide the support and the concrete sandwich resist local and global buckling in steel tube so it is used in bridge piers, high rise building and transmission tower in China. A new type of concrete-filled double skin steel tube CFDST with a varied cross section along the longitudinal direction which called tapered concrete filled double skin steel tube. The tapered CFDST is more economic than the straight CFDST and it can be useful in architectural requirement.

2. FINITE ELEMENT MODEL

2.1 General.

A nonlinear three-dimensional FE analysis has been modeled for circular tapered CFDST short columns under an axial load as shown in Fig. (1). The model consists of an inner tube, an outer tube, concrete sandwich and two end plates were used to cap both ends of the tapered CFDST short column to distribute the axial load on the inner and outer tubes besides the concrete sandwich. One-quarter of the circular tapered CFDST short column was modeled due to the symmetry of geometry and loading. The lower end of the columns was fixed, but the upper loaded end displacement in the direction of the applied load (Z-axis) was allowed. A uniform distributed load was applied incrementally at the top of the upper-end plate Fig. (1) using the displacement control approach together with the static RIKS method available in ABAQUS. The non-linear geometry parameter was available in static RIKS. The finite element meshes for tapered CFDST short columns are shown in Fig. (2). the inner and outer tubes were modeled as a solid element. For the concrete sandwich and the two end plates, four-node linear tetrahedron solid elements C3D4 were used. The initial imperfections effect on the strength of the tapered CFDST short columns was not considered in the FE modeling. Because the strength reduction of the thin-walled hollow tubes is not significant due to the delaying effect of the concrete core on the tube buckling as discussed by Tao et al. [2].

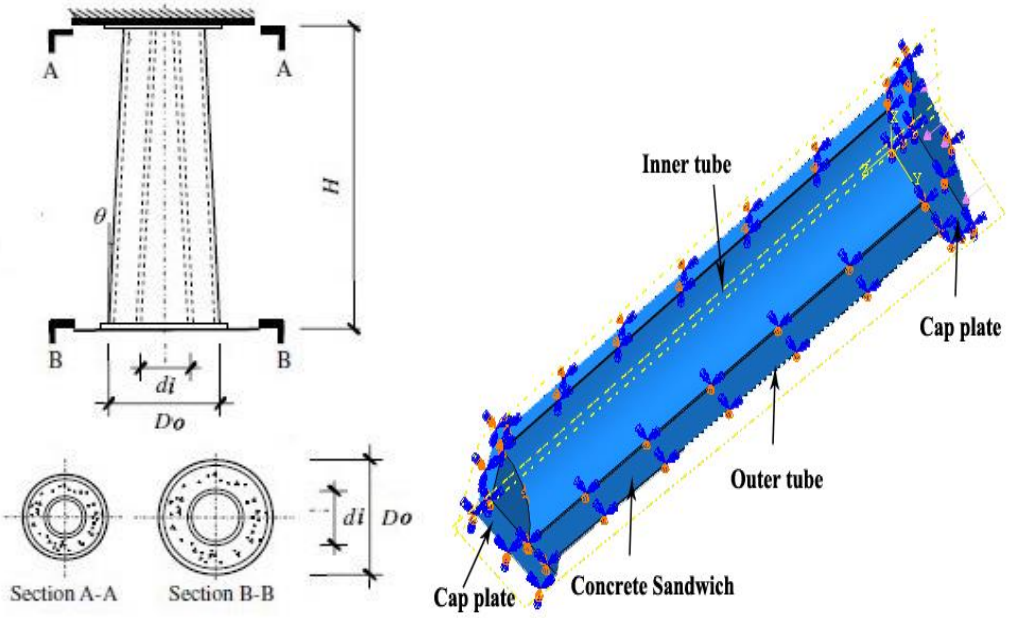

Figure 1 : front, top, bottom section view and ABAQUS model for quarter tapered (CFDST) short column

2.2 Finite Element Type and Mesh.

Typical finite element meshes for tapered CFDST columns are shown in Fig. (2). The 3D four-node linear tetrahedron solid elements **C3D4** was used to model both outer and inner tubes. A tapered CFDST short column with an outer steel tube of (D_{so}xt_{so}) and an inner steel tube of (d_{si}xt_{si}) was used for such analyses as shown in table (1). The concrete compressive strengths is (42 MPa) and the material properties of the outer and inner steel tube are in table (2). The approximate global size of mesh is 15 mm for outer and inner tubes, an approximate global size of the mesh is 30mm for concrete sandwich gives good results. For the concrete sandwich and the two end plates, the 3D four-node linear tetrahedron solid elements **C3D4** were used. The contact between the concrete sandwich and the outer tube, inner tube and end plates was applied as interaction as follow. The outer tube and inner tube surfaces were slave surfaces and the concrete surfaces were master surfaces and the friction was allowed in the initial step. And for the end plates and the concrete sandwich the end plates surfaces were master surfaces and the

concrete surfaces were slave surfaces and the friction was prevented in step-1. In case of modelling the outer and inner tubes as a solid element the contact between the inner or outer tube and both the end plates applied as interaction as follow the end plates surfaces were master surfaces and the tubes surfaces were slave surfaces and the friction was prevented in step-1. The friction coefficient between outer and inner steel tubes and the concrete sandwich was taken as 0.4 as suggested by Chang et al. [3].

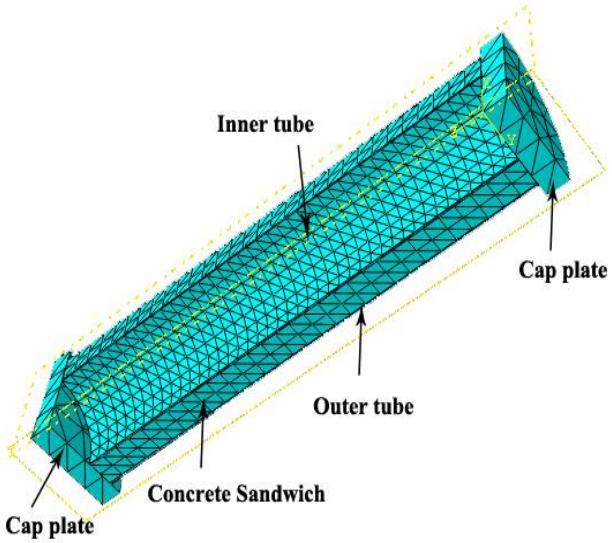

Figure 2: ABAQUS mesh for quarter tapered (CFDST) short column

2.3 Boundary Conditions and Load Applications.

Both ends of the tapered CFDST column were fixed but the displacement was allowed at the loaded end (the upper level of the cap) in the direction of the applied load (z-direction). The upper and lower connection of the concrete sandwich of the tapered CFDST short column were prevented from moving laterally, to prevent the elephant foot buckling at both ends of the columns. Due to modeling only a quarter of the column two symmetry planes is considered. A uniform distributed load was applied statically at the top of the upper-end plate using the displacement control. The load was applied incrementally using the modified RIKS method available in ABAQUS. The nonlinear geometry included dealing with the large displacement analysis.

2.4 Material.

a) Steel.

The steel material was modeled as the bilinear elastic-plastic stress-strain curve with linear strain hardening was used to simulate the steel material. The steel yield stress (f_{sy}), steel ultimate stress (f_{su}), the steel young modulus (E_s) and steel poison`s ratio are shown in table (2).

b) Concrete.

The inner tube of the CFDST columns provides restraint to the deformation of sandwiched concrete if the hollow section ratio ($d/(D-2t_o)$) is not larger than 0.80 Han et al. [5] providing the same behavior of the concrete in CFST columns. Therefore, a similar behavior as the core concrete in fully filled CFST columns was utilized in FE investigations [6, 7]. Fig (3) show the general stress - strain curve suggested by Liang and Fragomeni [8] to simulate the material behavior of confined concrete in circular CFDST columns The part OA of the stress–strain curve is represented using the equations proposed by Mander et al. [17] as.

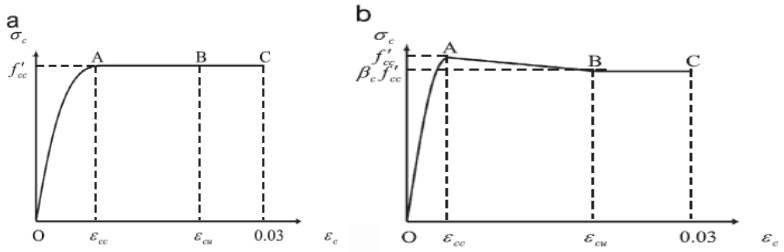

Figure 3: stress-strain curve for confined concrete in circular CFDST short columns:(a) D/te ≤40 and (b) 40<D/te≤150.

$$\sigma_c = \frac{f`_{cc}\lambda(\varepsilon_c/\varepsilon`_{cc})}{\lambda - 1 + (\varepsilon_c/\varepsilon`_{cc})^{\lambda}}$$

$$\lambda = \frac{E_c}{E_c - (f`_{cc}/\varepsilon`_{cc})}$$

In which (σ_c) denotes the longitudinal compressive concrete stress,$(f`_{cc})$ represents the compressive strength of confined concrete, $(\varepsilon_c)$ stands for the longitudinal compressive concrete strain and $(\varepsilon`_{cc})$ is the strain at $(f`_{cc})$. The Young's modulus of concrete (E_c) is given by ACI [9]. Where (γ_c) denotes the strength reduction factor proposed by Liang [10]. Hu et al. [12] and Tang et al. [13] have presented models for estimating the confining pressures on the concrete core in normal strength CFST columns. Based on their work, Liang and Fragomeni [8] proposed a confining pressure model for normal and high strength concrete confined by either a normal or high strength steel tube. The model given by Liang and Fragomeni [8] was adopted in the present study to determine the lateral confining pressures. The "Drucker–Prager yield criterion model" available in ABAQUS material library was adopted in the current investigation. This model defines the yield surface and the flow potential parameters for materials subjected to triaxial compressive stresses. To define the yielding stage of the passively confined concrete, two parameters (DRUCKER PRAGER and DRUCKER PRAGER HARDENING) were used. The linear Drucker–Prager model was used with associated flow and the isotropic rule. The material angle of friction (β) and the ratio of flow stress in triaxial tension to that in compression (K) were taken as 20 and 0.8, respectively, following the work conducted by Hu et al. [12]. Two parameters were used to determine the softening behavior of concrete in the post-peak stage of the concrete; namely (βc) and concrete strain (ε_{cu}) . As previously stated, the concrete strain (ε_{cu}) was taken as 0.02 based on experimental results of three-dimensional CFST columns [8].

2.5 VERIFICATION OF THE FINITE ELEMENT MODEL.

The finite element model was used to predict the behavior of tapered CFDST short columns tested by Qing et al. [4]. Two specimens were tested for each column. As shown in the table (3). The dimension of the inner tube and outer tube, columns height and tapered angle were given in table (1). the properties of the inner and outer tube were given in table (2).

Table 1: Experimental specimens

Specimen label	Outer tube D_{so} x t_{so} (mm x mm)		Inner tube d_{si} x t_{si} (mm x mm)		H (mm)	Θ(degree)
	Sec A-A	Sec B-B	Sec A-A	Sec B-B		
C 2	329x3.82	350x3.82	210x2.92	231x2.92	1050	0.57
C 3	308x3.82	350x3.82	189x2.92	231x2.92	1050	1.14
C 4	282x3.82	300x3.82	180x2.92	198x2.92	900	0.57
C 5	235x3.82	250x3.82	150x2.92	165x2.92	750	0.57

Table 2: Properties of the inner and outer steel tube

Type	Thickness (mm)	Yield Strength (N/mm^2)	Ultimate Strength (N/mm^2)	Elastic Modulus (N/mm^2)	Poisson`s ratio
Inner tube	2.92	396.5	530.7	$2.02x10^5$	0.295
Outer tube	3.82	439.3	508.5	$2.12x10^5$	0.307

The ultimate axial loads from the experimental tests $P_{UExp.}$ and the ultimate loads from the finite element analysis $P_{UFE.}$ Of the tapered CFDST, short columns and the comparison of finite element results with the experimental results were shown in table (3)the the mean value and the standard deviation of the $P_{UFE.}/P_{UExp.}$were 0.98 and 0.0139 respectively as shown in table (3).

Table 3: Comparisons between finite element and an experimental ultimate load of CFDST columns.

Specimen label	$P_{UExp.}$ [kN]	P_{UFE} [kN]	$P_{UFE}/P_{UExp.}$
C 2-1	4942	4881	0.99
C 2-2	4921		0.99
C 3-1	4569	4497	0.98
C 3-2	4600		0.98
C 4-1	3874	3829	0.99
C 4-2	4048		0.95
C 5-1	3090	3010	0.97
C 5-2	3116		0.97
Average			**0.98**
Standard deviation			**0.0139**

Load versus strain relationships of tapered CFDST short columns with inner and outer tubes as solid elements are shown in Fig. (4). the accurate model was that the outer and inner tubes were solid elements that give accurate results.

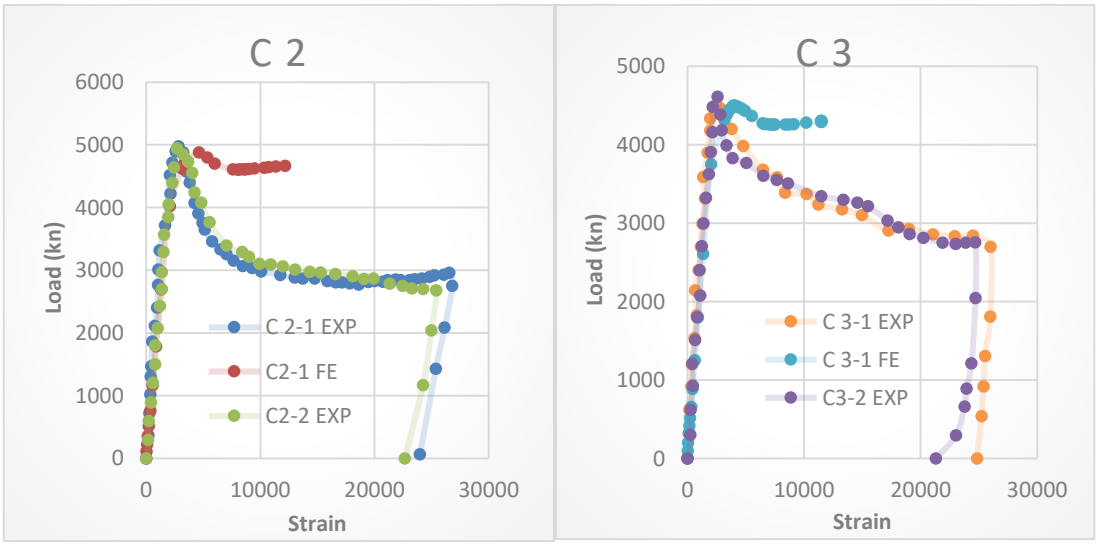

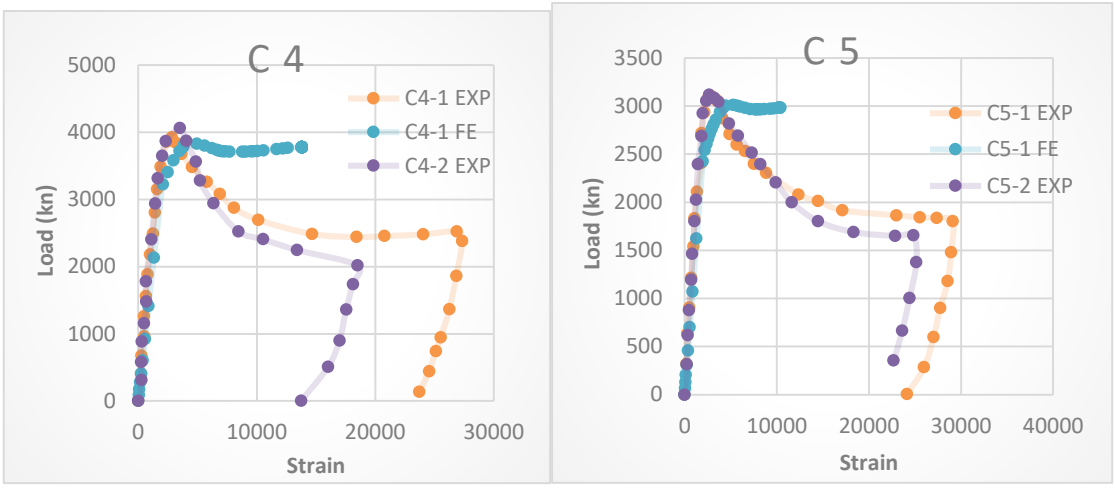

Figure 4: load versus strain relations of tapered CFDST short columns solid elements

3. PARAMETRIC STUDY.

3.1 General.

Finite element analyses for 84 model in 22 group were employed to carry out a parametric study to investigate carefully the behavior of tapered concrete filled double skin steel tubular columns (CFDST) under the effect of varied parameters. The column`s height (H) was taken three times the bigger diameter of the outer tube (D_o) to avoid the effect of column slenderness. The dimensions of the columns and the concrete strength are shown in tablthe e (4). The diameter of the outer steel tube varied from 200mm to 400mm as shown in table (4). The concrete compressive strength varied between 25 MPa to 40 MPa. The ratio of the internal tube thickness-to-outer tube thickness (t_i/t_o) varied from 0.63 to 1. The tapered angle (θ) varied from 0.5degree to 1 degree. The ratio of the diameter of internal tube-to-the diameter of the outer tube (d_i/D_o) varied from 0.25 to 0.88 as shown in table (4).

Table 4: Properties of the specimens columns.

Groups	Specimens label	D_o	d_i	$\frac{d_i}{D_o}$	t_o	t_i	$\frac{t_i}{t_o}$	θ	H	*fc*
G1	C1	200	100	0.50	8	4	0.50	0.50	600	25
	C2	200	100	0.50	8	4	0.50	0.50	600	30
	C3	200	100	0.50	8	4	0.50	0.50	600	35
	C4	200	100	0.50	8	4	0.50	0.50	600	40
G2	C5	200	100	0.50	8	4	0.50	0.75	600	25
	C6	200	100	0.50	8	4	0.50	0.75	600	30
	C7	200	100	0.50	8	4	0.50	0.75	600	35
	C8	200	100	0.50	8	4	0.50	0.75	600	40
G3	C9	200	100	0.50	8	4	0.50	1.00	600	25
	C10	200	100	0.50	8	4	0.50	1.00	600	30
	C11	200	100	0.50	8	4	0.50	1.00	600	35
	C12	200	100	0.50	8	4	0.50	1.00	600	40
G4	C13	200	100	0.50	8	5	0.63	0.75	600	35
	C14	200	100	0.50	8	6	0.75	0.75	600	35
	C15	200	100	0.50	8	8	1.00	0.75	600	35
G5	C16	250	125	0.50	8	4	0.50	0.50	750	25

	C17	250	125	0.50	8	4	0.50	0.50	750	30
	C18	250	125	0.50	8	4	0.50	0.50	750	35
	C19	250	125	0.50	8	4	0.50	0.50	750	40
G6	C20	250	125	0.50	8	4	0.50	0.75	750	25
	C21	250	125	0.50	8	4	0.50	0.75	750	30
	C22	250	125	0.50	8	4	0.50	0.75	750	35
	C23	250	125	0.50	8	4	0.50	0.75	750	40
G7	C24	250	125	0.50	8	4	0.50	1.00	750	25
	C25	250	125	0.50	8	4	0.50	1.00	750	30
	C26	250	125	0.50	8	4	0.50	1.00	750	35
	C27	250	125	0.50	8	4	0.50	1.00	750	40
G8	C28	250	125	0.50	8	5	0.63	0.75	750	35
	C29	250	125	0.50	8	6	0.75	0.75	750	35
	C30	250	125	0.50	8	8	1.00	0.75	750	35
G9	C31	300	150	0.50	8	4	0.50	0.50	900	25
	C32	300	150	0.50	8	4	0.50	0.50	900	30
	C33	300	150	0.50	8	4	0.50	0.50	900	35
	C34	300	150	0.50	8	4	0.50	0.50	900	40
G10	C35	300	150	0.50	8	4	0.50	0.75	900	25
	C36	300	150	0.50	8	4	0.50	0.75	900	30
	C37	300	150	0.50	8	4	0.50	0.75	900	35
	C38	300	150	0.50	8	4	0.50	0.75	900	40
G11	C39	300	150	0.50	8	4	0.50	1.00	900	25
	C40	300	150	0.50	8	4	0.50	1.00	900	30
	C41	300	150	0.50	8	4	0.50	1.00	900	35
	C42	300	150	0.50	8	4	0.50	1.00	900	40
G12	C43	300	150	0.50	8	5	0.63	0.75	900	35
	C44	300	150	0.50	8	6	0.75	0.75	900	35
	C45	300	150	0.50	8	8	1.00	0.75	900	35
G13	C46	350	175	0.50	8	4	0.50	0.50	1050	25
	C47	350	175	0.50	8	4	0.50	0.50	1050	30
	C48	350	175	0.50	8	4	0.50	0.50	1050	35
	C49	350	175	0.50	8	4	0.50	0.50	1050	40
G14	C50	350	175	0.50	8	4	0.50	0.75	1050	25
	C51	350	175	0.50	8	4	0.50	0.75	1050	30
	C52	350	175	0.50	8	4	0.50	0.75	1050	35
	C53	350	175	0.50	8	4	0.50	0.75	1050	40
G15	C54	350	175	0.50	8	4	0.50	1.00	1050	25
	C55	350	175	0.50	8	4	0.50	1.00	1050	30
	C56	350	175	0.50	8	4	0.50	1.00	1050	35
	C57	350	175	0.50	8	4	0.50	1.00	1050	40
G16	C58	350	175	0.50	8	5	0.63	0.75	1050	35
	C59	350	175	0.50	8	6	0.75	0.75	1050	35
	C60	350	175	0.50	8	8	1.00	0.75	1050	35
G17	C61	400	200	0.50	8	4	0.50	0.50	1200	25
	C62	400	200	0.50	8	4	0.50	0.50	1200	30
	C63	400	200	0.50	8	4	0.50	0.50	1200	35
	C64	400	200	0.50	8	4	0.50	0.50	1200	40
G18	C65	400	200	0.50	8	4	0.50	0.75	1200	25
	C66	400	200	0.50	8	4	0.50	0.75	1200	30
	C67	400	200	0.50	8	4	0.50	0.75	1200	35
	C68	400	200	0.50	8	4	0.50	0.75	1200	40
G19	C69	400	200	0.50	8	4	0.50	1.00	1200	25
	C70	400	200	0.50	8	4	0.50	1.00	1200	30
	C71	400	200	0.50	8	4	0.50	1.00	1200	35

	C72	400	200	0.50	8	4	0.50	1.00	1200	40
G20	C73	400	200	0.50	8	5	0.63	0.75	1200	35
	C74	400	200	0.50	8	6	0.75	0.75	1200	35
	C75	400	200	0.50	8	8	1.00	0.75	1200	35
G21	C76	300	100	0.33	8	4	0.50	0.75	900	35
	C37	300	150	0.50	8	4	0.50	0.75	900	35
	C77	300	200	0.67	8	4	0.50	0.75	900	35
	C78	300	225	0.75	8	4	0.50	0.75	900	35
	C79	300	250	0.83	8	4	0.50	0.75	900	35
G22	C80	400	100	0.25	8	4	0.50	0.75	1200	35
	C67	400	200	0.50	8	4	0.50	0.75	1200	35
	C81	400	250	0.63	8	4	0.50	0.75	1200	35
	C82	400	300	0.75	8	4	0.50	0.75	1200	35
	C83	400	325	0.81	8	4	0.50	0.75	1200	35
	C84	400	350	0.88	8	4	0.50	0.75	1200	35

3.2 Effect of Concrete Compressive Strength (fc).

The concrete compressive strength (*fc*) varied from 25Mpa to 40Mpa. It takes the values 25Mpa, 30Mpa, 35Mpa, and 40Mpa for each group. The other parameters are constant as shown in table (4). Fig (5), fig (6) and fig (7) show the axial load-strain curve for each group. From fig (5), fig (6) and fig (7) it was found that increasing the concrete compressive strength (*fc*) increases the ultimate axial strength for the tapered (CFDST) because of the increase of confinement effect. Ductility increases with increasing the compressive strength of concrete. On the other hand, the initial stiffness remains constants for all values of (*fc*).

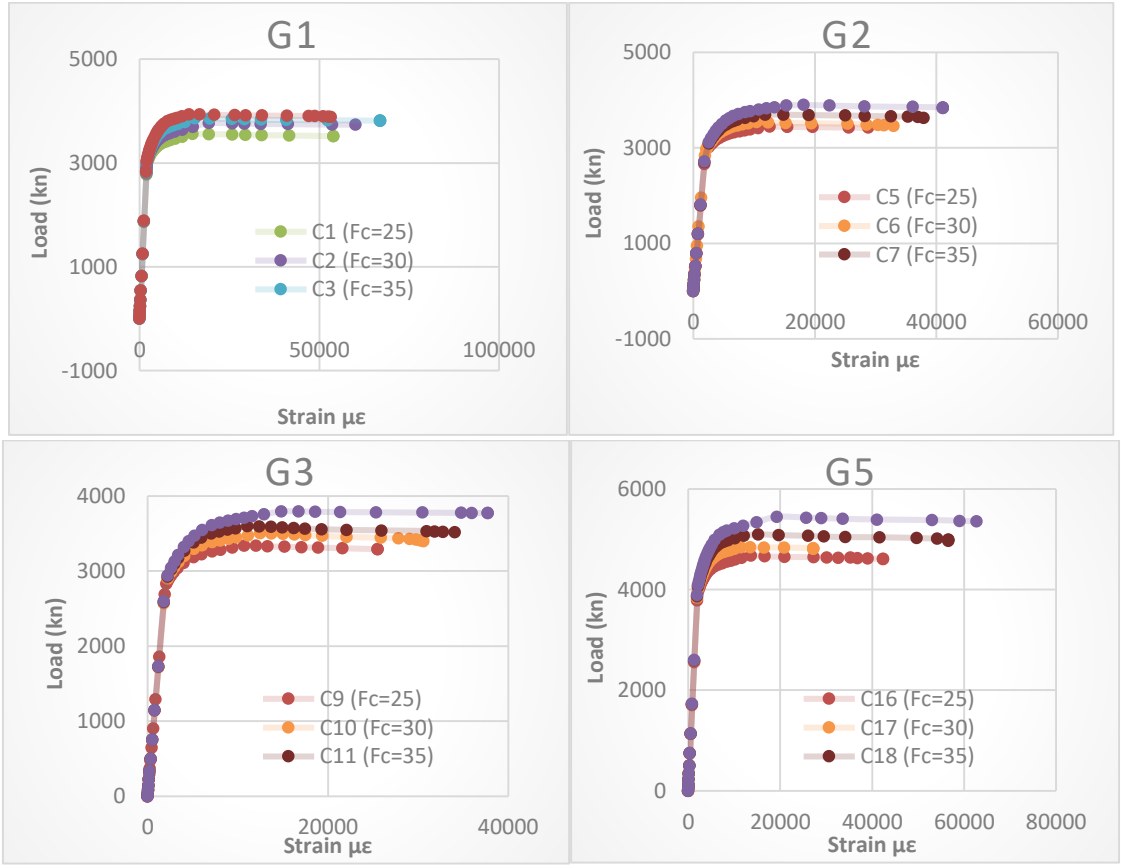

Figure 5: load-strain curves for the effect of concrete compressive strength (fc) for groups G1, G2, G3, and G5.

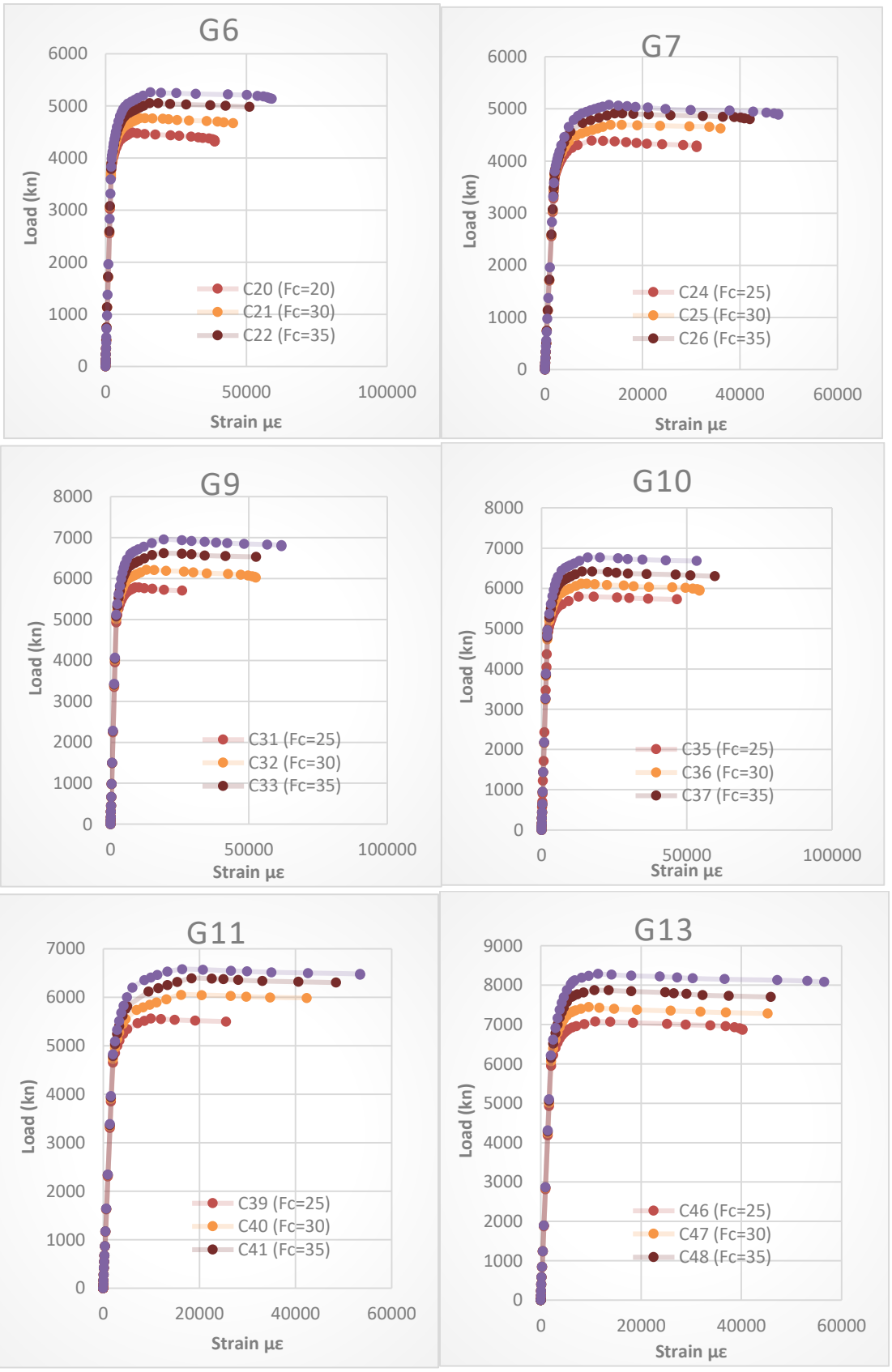

Figure 6: load-strain curves for the effect of concrete compressive strength (fc)c for groups G6, G7, G9, G10, G11, and G13.

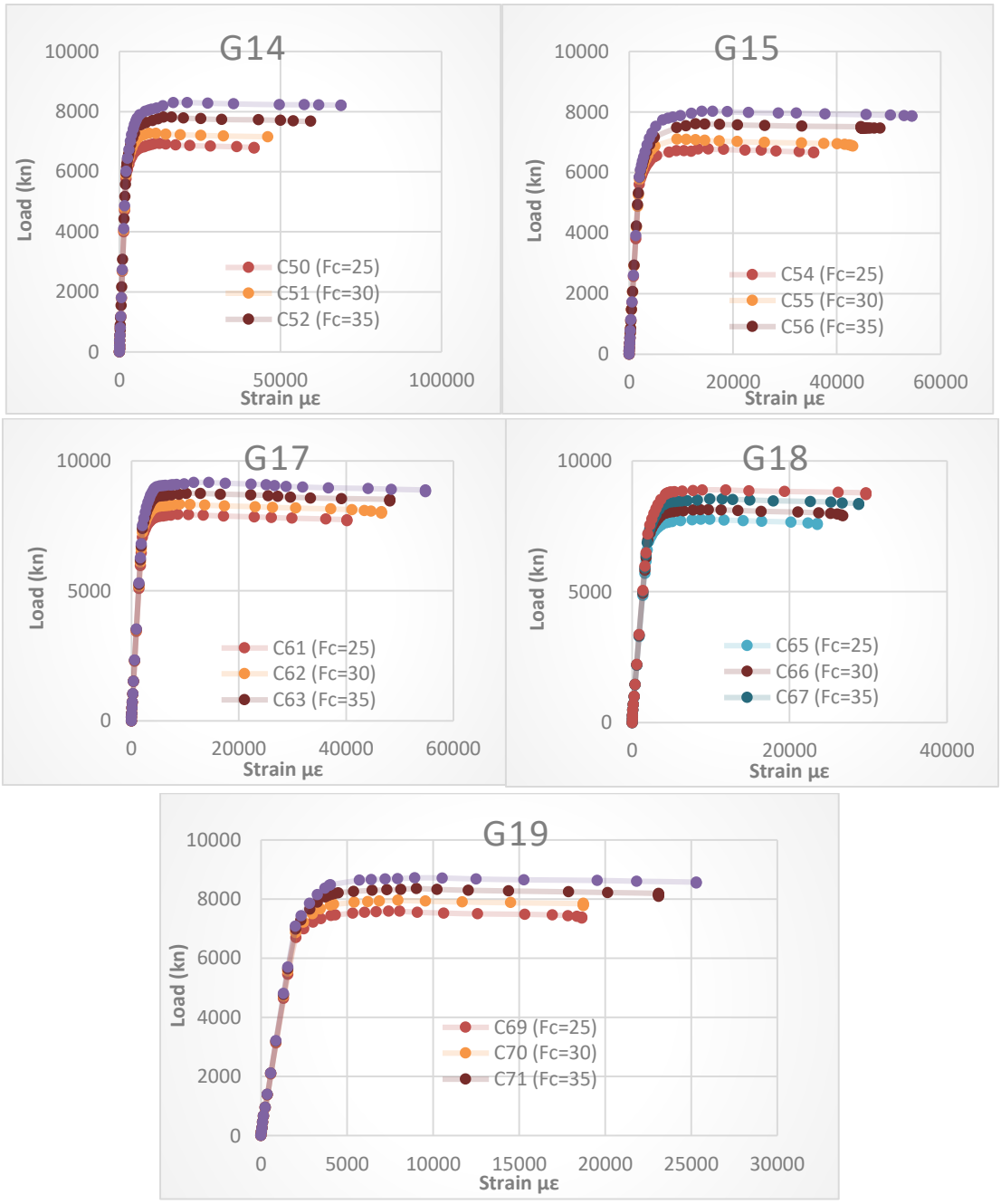

Figure 7: load-strain curves for the effect of concrete compressive strength (fc) for groups G17, G18 and G 19.

3.3 Effect of the internal Tube Thickness to The outer Tube (t_i/t_o).

The ratio of the internal tube thickness to the outer tube thickness (t_i/t_o) varied from 0.63 to 1 and take the values 0.36, 0.75, 1 with constant (t_o)that equal 8mm and (t_i) take the values 5mm, 6mm and 8mm. the other parameters are constant. From the load-strain curves shown in fig (8) it is clear that increasing (t_i/t_o) ratio increases the ultimate axial strength for the (CFDST) because of the increase in (t_i/t_o) ratio due to the increase in (t_i) making more support to the concrete sandwich which increase the ultimate axial strength for the tapered (CFDST). It can be observed from the results that the changing in values of (t_i/t_o) has no effects on ductility. Moreover, the initial stiffness is constant for all values of (t_i/t_o).

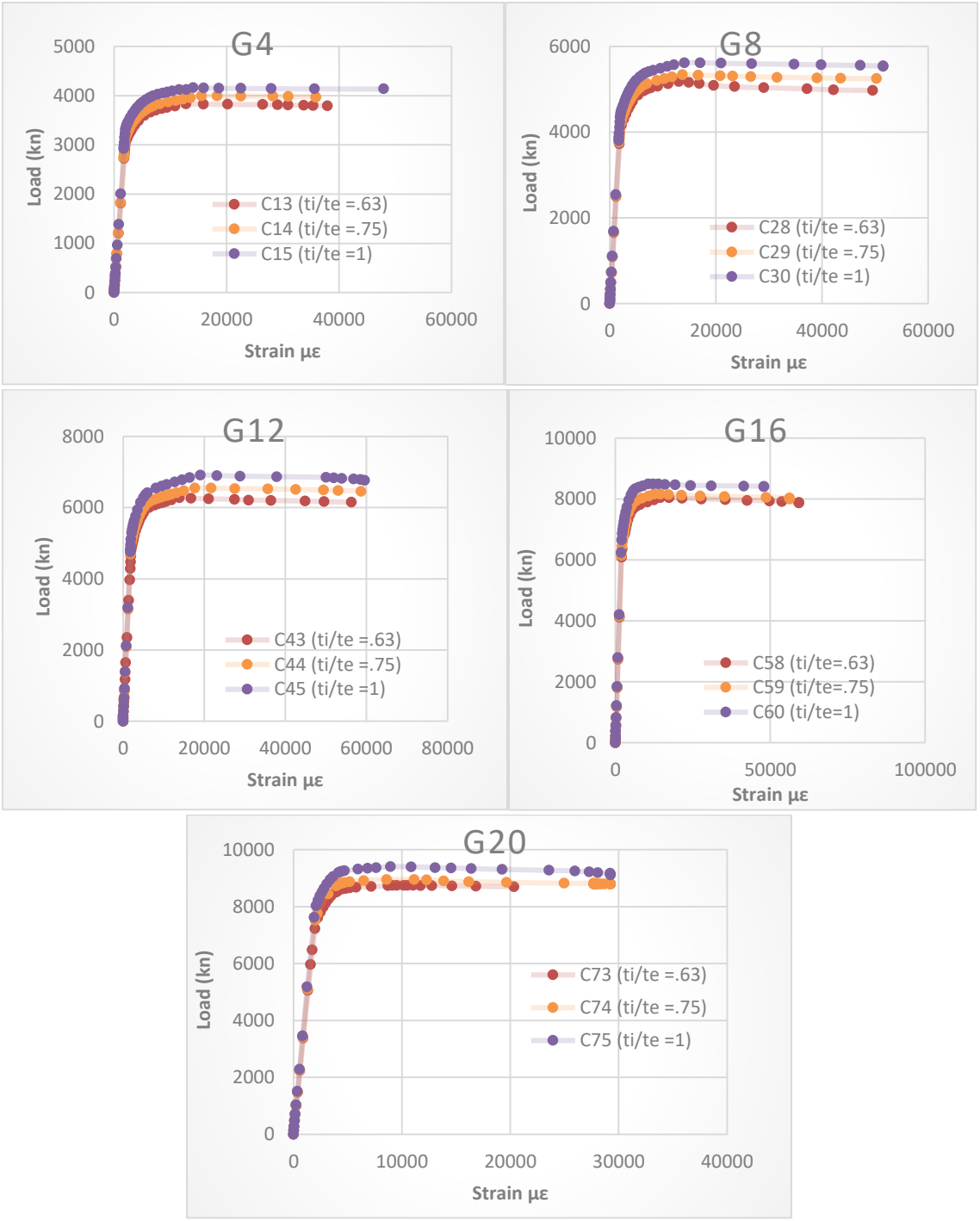

Figure 8: load-strain curves for the effect of (ti/to).

3.4 Effect of The internal Tube Diameter to The outer Tube Diameter (d_i/D_o).

The internal tube diameter to the outer tube diameter (d_i/D_o) varied and take the values 0.33, 0.5, 0.67, 0.75, 0.83 for the outer tube diameter (D_o)=300mm (Group G21) and take the values 0.25, 0.5, 0.63, 0.75, 0.81, 0.88 for the outer tube diameter (D_o)=400mm (Group G22). The other parameters are constant. From the load-strain curves shown in fig (9) it is clear that increasing (d_i/D_o) ratio decreases the ultimate axial strength for the (CFDST).). It can be observed from the results that the changing in values of (d_i/D_o) has no effects on ductility. Moreover, the initial stiffness is constant for all values of (d_i/D_o).

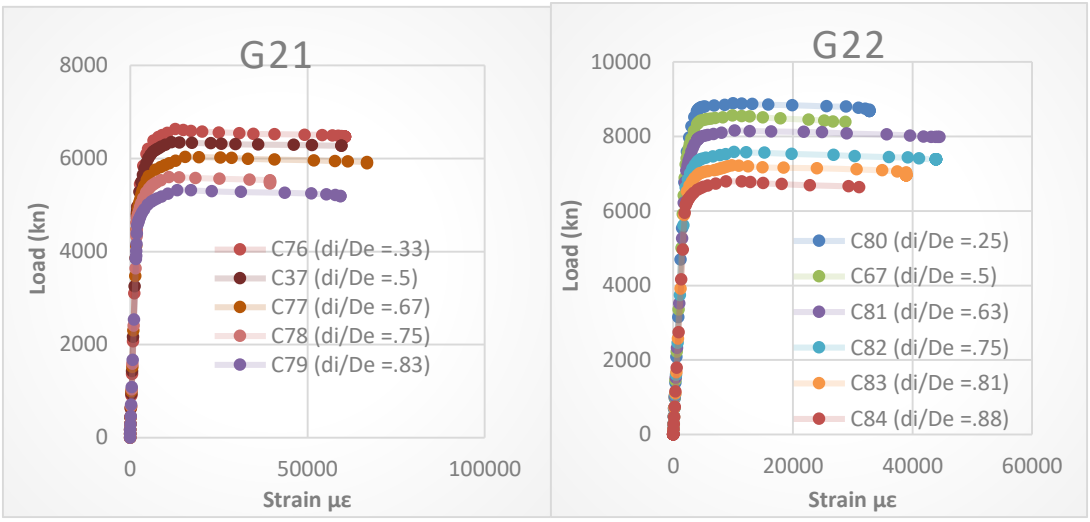

Figure 9: load-strain curves for the effect of (di/Do).

3.5 Effect of Tapered Angle (θ).

The tapered angle varied and take the values 0.5, 0.75, 1degree. The internal tube thickness to outer tube thickness (t_i/t_o) is constant and equal (0.5). The internal tube diameter to outer tube diameter (d_i/D_o) is constant and equal (0.5). The concrete compressive strength (*fc*) is constant for the same charts and equal 35Mpa. the biggest cross section (sec B-B) is constant and the smallest cross section (sec A-A) varies with the variation of tapered angle as shown in fig (10). From the load-strain curves shown in fig (11) it is clear that increasing tapered angle (θ) decreases the ultimate axial strength for the (CFDST).

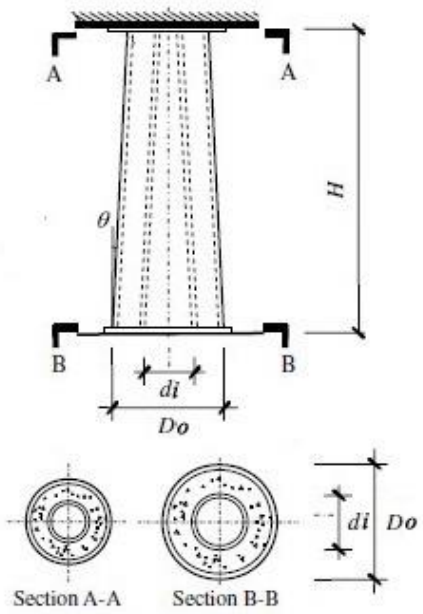

Figure (10): Elevation and cross section for tapered CFDST columns.

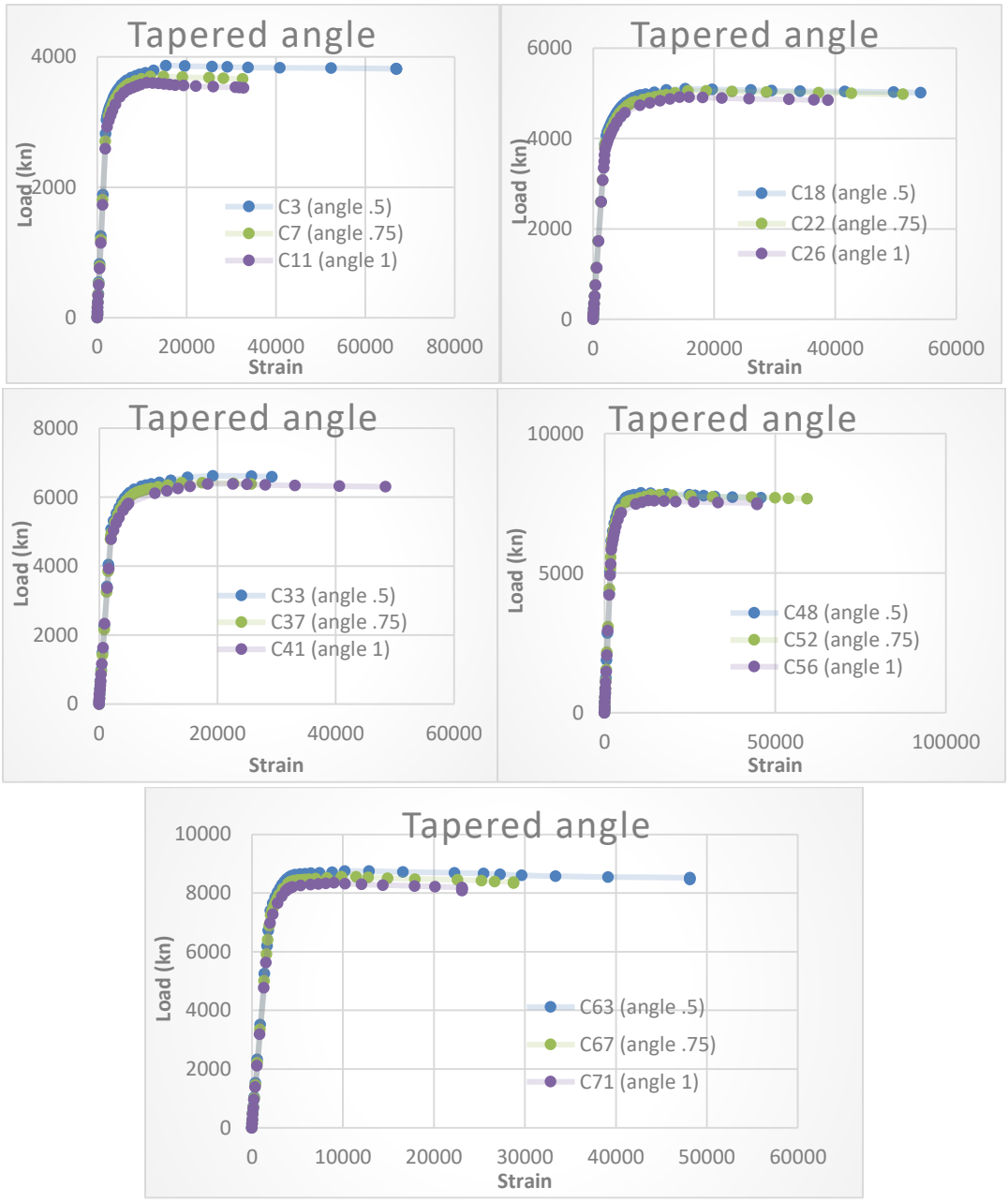

Figure (11): load-strain curves for the effect of tapered angle (θ).

4. DESIGN STRENGTH

There are several advanced design methods that calculate the compressive strength of the CFDST columns such as ACI code [18], Uenaka et al. [19], Han et al. [20,21], Yu et al. [22], Hassanein et al. [23] and Hassanein new proposed design method. Hassanein et al. [24]. The previous advanced design methods that calculate the compressive strength of the CFDST columns can be used to calculate the compressive strength of the Tapered-CFDST columns with different tapered angles. For the tapered CFDST short columns, the strength of the column is related to the smallest section where the failure may probably happen so the smallest section is used in the calculation of the compressive strength [4].

5. CONCLUSIONS

- Increasing the concrete compressive strength (*fc*) increases the ultimate axial strength for the (CFDST) because of the increase of the confinement effect. Ductility increases with increasing

the compressive strength of concrete. On the other hand, the initial stiffness remains constants for all values of (*fc*)**.**

- Increasing (t_i/t_o) ratio increases the ultimate axial strength for the (CFDST).
- increasing (d_i/D_o) ratio decreases the ultimate axial strength for the (CFDST).). It can be observed from the results that the changing in values of (d_i/D_o) has no effects on ductility. Moreover, the initial stiffness is constant for all values of (d_i/D_o).

- The tapered angle varied and take the values 0.5, 0.75, 1 degree. increasing tapered angle (θ) decreases the ultimate axial strength for the (CFDST).

6 REFERENCES.

[1] Hassanein MF, Kharoob OF, Liang QQ. Behavior of circular concrete-filled lean duplex stainless steel carbon steel tubular short columns. Engineering Structures 2013;56:83–94.
[2] Tao Z, Uy B, Han LH, Wang ZB. Analysis and design of concrete-filled stiffened thin-walled steel tubular columns under axial compression. Thin-Walled Structures 2009;47(12):1544–56.
[3] Young B, Ellobody E. Experimental investigation of concrete-filled cold- formed high strength stainless steel tube columns. Journal of Constructional Steel Research 2006;62(5):484–92.
[4] Wei, Qing, et al Behavior of tapered concrete-filled double skin steel tubular (CFDST) stub columns thin-wall structures 2012;57:37-48.
[5] Tao Z, Han L-H, Zhao X-L. Behavior of concrete-filled double skin (CHS inner and CHS outer) steel tubular stub columns and beam-columns. Journal of Constructional Steel Research 2004;60(8):1129–58.
[6] Han L-H, Huang H, Zhao X-L. Analytical behavior of concrete-filled double skin steel tubular (CFDST)beam-columns under cyclic loading. Thin-Walled Structures2009;47:668–80.
[7] Li W, Han L-H, Zhao X-L. Axial strength of concrete-filled double skin steel tubular (CFDST) columns with preload on steel tubes. Thin-Walled Structures 2012;56:9–20.
[8] Liang QQ, Fragomeni S. Nonlinear Analysis of circular concrete-filled steel tubular short columns under axial loading. Journal of Constructional Steel Research 2009;65(12):2186–96.
[9] ACI-318. Building code requirements for reinforced concrete. Detroit (MI): ACI; 2002.
[10] Liang QQ. Performance-based analysis of concrete-filled steel tubular beam- columns. Part I: theory and algorithms. Journal of Constructional Steel Research 2009;65(2):363–73.
[11] Richart FE, Brandtzaeg A, Brown RL. A study of the failure of concrete under combined compressive stresses. Bull. 185. Champaign (III): University of Illinois. Engineering Experimental Station; 1928.
[12] Hu HT, Huang CS, Wu MH, Wu YM. Nonlinear analysis of axially loaded concrete-filled tube columns with confinement effect. Journal of Structural Engineering, ASCE2003;129(10):1322–9.
[13] Tang J, Hino S, Kuroda I, Ohta T. Modeling of stress-strain relationships for steel and concrete in concrete filled circular steel tubular columns. Steel Construction Engineering, JSSC1996;3(11):35–46.
[14] Ellobody E, Young B. Design, and behavior of concrete-filled cold-formed stainless steel tube columns. Engineering Structures 2006;28:716–28.
[15] Hassanein MF, Kharoob OF, Liang QQ. The behavior of Circular concrete-filled lean duplex stainless steel tubular short columns. Thin-Walled Structures 2013;68:113–23.
[16] Hassanein MF, Kharoob OF, Liang QQ. The behavior of circular concrete-filled lean duplex stainless steel-carbon steel tubular short columns. Engineering Structures 2013;56:83–94.
[17] Mander JB, Priestley MJN, Park R. Theoretical stress-strain model for confined concrete. Journal of Structural Engineering, ASCE 1988;114(8):1804–26.
[18] ACI-318. Building code requirements for reinforced concrete. Detroit (MI): ACI; 2002.
[19] Uenaka K, Kitoh H. Sonoda K. Concrete filled double skin circular stub columns under compression.Thin-WalledStruct2010;48:19–24.
[20] Han L-H, Tao Z, Huang H, Zhao XL. Concrete-filled double-skin (SHS outer and CHS inner) steel tubular beam-columns. Thin-Walled Structures 2004; 42(9):1329–55.
[21] Han L-H, Ren Q-X, Wei L. Tests on stub stainless steel–concrete–carbon steel double-skin tubular(DST) columns. J Constr Steel Res 2011;67:437–52.
[22] Yu M, Zha X, Ye J, Li Y. A unified formulation for circle and polygon concrete-filled steel tube columns under axial compression. Eng Struct 2013;49:1–10.